IEEE Access
Multidisciplinary | Rapid Review | Open Access Journal

Received December 2, 2017, accepted January 25, 2018, date of publication March 28, 2018, date of current version May 24, 2018.

Digital Object Identifier 10.1109/ACCESS.2018.2810265

Microwave Excitation of Crystalline Energetic Composites

MICHAEL CHEN, (Student Member, IEEE), MOHAMMED A. ZIKRY, AND MICHAEL B. STEER, (Fellow, IEEE)
North Carolina State University, Raleigh, NC 27695, USA

Corresponding author: Michael Chen (mchen8@ncsu.edu)

This work was supported by the U.S. Office of Naval Research as a Multi-Disciplinary University Research Initiative on Sound and Electromagnetic Interacting Waves under Grant N00014-10-1-0958.

ABSTRACT Hotspots produced by microwaves radiating into an energetic composite of RDX crystals and an estane binder are examined using transient electromagnetic (EM) and coupled EM-thermal analyses. Hotspots, localized regions where energetic activity is likely to initiate, manifest as regions of peak electric field or high temperature. Stress caused by these high fields and temperatures may result in molecular breakdown, creating a chain reaction leading to the release of chemical energy via deflagration (burning and melting) in the absence of a mechanical shock wave. High peak electric fields up to three times higher than the incident field result from subwavelength scattering and occur near crystalline surfaces while peak temperatures occur in the binder, with both generally coinciding at the binder-RDX interface. Abstractions enable materials to be modeled with crystals having an average characteristic dimension of 100 μm. With an incident field of 1 MV/m the peak electric field in the composite was 2.9 MV/m and peak temperature increased by 75 K in the binder and 65 K in the RDX after 3.7 ms. The RDX fill factor of the composite was 37%, typical of an improvised explosive.

INDEX TERMS Electromagnetic loading, granular materials, composites, directed energy, subwavelength scattering, energetic materials, dielectric heating, high power microwaves, FDTD.

I. INTRODUCTION

Investigation into the electromagnetic (EM) excitation of energetic materials has gained traction as it has been demonstrated that standoff detonation, and more significantly, deflagration of energetic materials can be achieved using directed EM radiation [1]–[4]. This capability has applications in remote detonation and disarmament of explosives, particularly improvised explosive devices (IEDs), presenting the possibility of a ranged neutralization system able to avoid the danger of explosion. Such a system could sweep an area for possible danger, simultaneously locating and neutralizing threats in a nondestructive manner.

It has been suggested that initiation by EM excitation is due to the localized shifting of electric charges by electric fields, weakening chemical bonds within the material at the molecular level and facilitating their breakage [5], [6]. This effect is augmented by heating of the material through the dielectric loss of the EM wave [7], [8]. Increased levels of both temperature and charge gradients in these materials have also been shown to reduce initiation thresholds for excitation via shock or acoustic sources [6], [9]. Thus, it is important that any potential EM or EM-hybrid initiation/neutralization system seeks to maximize peak electric field and temperature rise by EM–induced heating.

Experimental investigations of EM standoff initiation often involve the use of laser sources [2], [4], [10], [11]. Lasers, known for their high intensities, are an attractive choice to maximize the aforementioned charge gradients and heating. Laser beams are typically highly focused with sub-millimeter beamwidths, and over distance beam spreading rapidly reduces the observed power density. Thus, the effective range demonstrated in experiments is often very low [12] or requires a laboratory environment with a focusing system of mirrors and lenses [2], limiting their applicability in real world situations. In addition, EM waves at laser frequencies (750 nm – 10 μm) have poor penetrative capabilities and are easily blocked by a covering or the ground, limiting their efficacy against buried or otherwise hidden devices.

In contrast to lasers, microwaves are known for their ability to penetrate many common mediums relatively unimpeded, including many soil types [13], [14]. Though most effective below 10 GHz, attenuation rates remain reasonable

up to 100 GHz. Recent developments have demonstrated gigawatt–level pulsed microwave sources in the 10 GHz range [15]. The comparatively high range and penetration of directed microwave beams over those of lasers offer a distinct advantage in the neutralization of buried and hidden explosives.

The penetrative properties of microwaves come with drawbacks. In particular, the relatively low loss of microwaves limits the volumetric heat transferred to the material. Previous theoretical and experimental investigations using microwaves have demonstrated substantially lower heating rates than those with lasers [1], [3], [16], resulting in reduced reliability of initiation. To ensure the viability of a microwave excitation system, both the reliability and time to event must be improved. The end goal, the development of a microwave system capable of reliably causing deflagration of explosives at a safe distance, depends on greater insight into the underlying phenomena of energy localization in granular materials such as improvised explosives. To more effectively exploit the microwave excitation of energetic materials, the precise behavior of the EM fields within the scattering medium must be understood.

One common technique for the analysis of microwaves propagation through granular composites is the use of effective medium characterizations [17], [18]. This appears to be a promising method, as inclusions are typically on the scale of tens to hundreds of microns in size. At 16.5 GHz, this compares to a wavelength of 1.82 cm in vacuum or 1.14 cm in RDX and appears sufficiently small such that subwavelength effects could be ignored. However, initiation of detonation or deflagration may occur over the course of nanoseconds, and has been traced to behavior at the molecular level [19], with peak fields shown to be on the micron-scale in size at the surfaces of crystals or their internal voids [3], [20], [21]. Thus, it is the peak electric field, specifically at the surface of the inclusions themselves, which is important. While an analysis using effective permittivity may capture bulk effects, field behavior at the inclusion level will be overlooked. This investigation therefore focuses on sub-inclusion scale field effects within the medium itself.

The purpose of this paper is to determine the peak electric field and maximum heating that occurs in a composite explosive material for an incident electric field with a magnitude of 1 MV/m, an appreciable percentage of the breakdown condition in air (3 MV/m). This provides information with which the feasibility of a standoff microwave neutralization system may be determined. Section 2 describes approaches used to develop insight into the excitation of explosives using indirect means such as directed acoustic and EM beams and then summarizes approaches for EM modeling of three-dimensional (3D) granular structures. Section 3 describes the simulation environment used in the study presented in this paper, covering the generation of the simulated structure itself, the EM simulation method, and the EM-thermal coupling technique. Section 4 is a discussion and the impact of the excitation on the medium is described and analyzed. Finally, conclusions of the study are presented.

II. APPROACH

Ideally, physical insights into the behavior of energetic systems would be obtained through observation and measurements. However, experimentation on such materials is inherently dangerous and difficult to record. To minimize this danger, experiments may use small samples of material which only burn rather than explode [1], [9]. Indirect forms of measurement may also be employed, as in situ electric field measurements within an exploding energetic material are impractical. Such indirect data may range from surface temperature measurements using infrared cameras [1], [12], [22], to the analysis of acoustic data recorded during the explosive event [23].

System-level measurements cannot describe the mechanisms behind detonation and deflagration, which requires investigations at fine resolutions in both space and time. It is important that highly localized effects in both field and temperature are recorded, as changes that occur in very small windows of space and time can incite initiation in energetic materials. Proper modeling of field extrema caused by subwavelength scattering and geometries are therefore crucial to understanding these events.

There have been previous investigations which have utilized simulations to study temperature and field behavior at high resolution in these materials. Brown and Zikry [8] performed an extensive analysis to examine the temperature change caused by an array of coupled stress factors, including laser excitation. Pickles *et al.* [17], [18] examined effective permittivity properties to determine the potential of composite energetic materials to absorb and retain energy.

However, due to the complicated nature of these mediums, inclusions may be on the scale of microns while the composite structure may have a volume of cubic centimeters, all investigations must employ abstractions. Abstractions include the reduction to two-dimensions [3], [8], significant simplification in the shape of the inclusions [3], or the de-emphasis of inclusion-scale scattering in favor of a bulk analysis [17], [18].

This work performs full-wave 3D EM simulations while maintaining the contribution of sub-inclusion scale field variations. With inclusions having a characteristic linear dimension of 100 μm the spatial resolution was 4 μm. The time resolution is on the scale of picoseconds. Abstraction of the inclusions as randomly oriented cubes is still necessary, and a method previously shown to faithfully represent the correct electric field localization will be used [21]. In addition, the dielectric heating of the system must be modeled at the same space scale. Both the EM and thermal simulations are performed in the time domain, allowing for peak field values to be recorded in time. This allows for an instantaneous peak value to be recorded rather than a value average over a time window, reducing the possibility that critical peaks are not captured due to lack of time resolution.

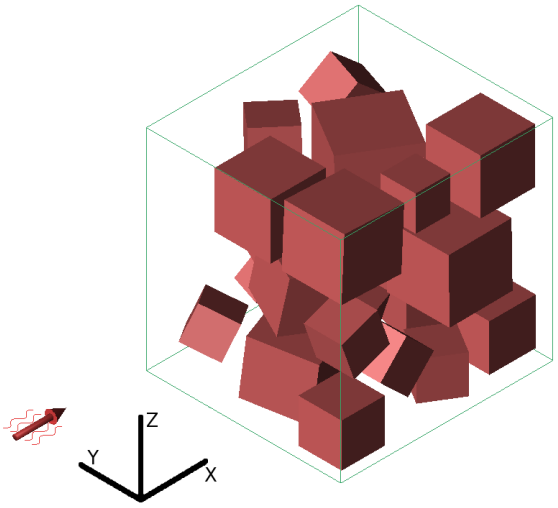

FIGURE 1. Simulation structure (shown here in xFDTD).

TABLE 1. Physical parameters of RDX and estane binder.

	RDX [8], [16]	Estane [8]
Density, ρ (kg/m^3)	1820	1190
Specific heat, c_p (J/(kg·K))	1260	1500
Thermal conductivity, κ (W/(m·K))	0.29	0.14
Real relative permittivity, $\varepsilon_{r,\text{real}}$	2.54	1.13
Imaginary relative permittivity, $\varepsilon_{r,\text{imag}}$	0.003	0.0117

III. METHOD

A. METHODS-MEDIUM

The simulation structure used throughout this investigation is illustrated in Fig. 1. The medium is modeled as a cubic block measuring 1.3 mm by 1.1 mm by 1.05 mm, populated with randomly oriented cubical inclusions, each varying in side length from 70 μm to 130 μm. The structure is generated by a C++ script using the Bullet physics library effectively realizing a computer game, as described in [21]. Such a structure of cubes has been shown to display comparable levels of field localization to that of more complex structures, substantially improving upon a commonly used abstraction with a spherical inclusion model [21]. Cubical crystals of randomly determined size are dropped into a box similar to that shown in Fig. 1, and the entire system is shaken to distribute the crystals throughout. Each crystal is given a randomly defined collision box which extends up to 10 μm beyond its physical dimensions, preventing an orderly structure from forming. The material of the inclusions is RDX and the binder is an estane polymer, the EM and thermal material properties of which are presented in Table 1. The overall volume fraction of the RDX inclusions is approximately 37%, which is typical of homemade explosives. The simulation process is divided into two separate portions, an EM simulation of a microwave excitation, and a thermal simulation of the medium's thermal response to the EM behavior.

B. METHODS-ELECTROMAGNETICS

The EM and thermal portions of the simulation are separated, with the EM analysis performed first. These simulations are performed in Remcoms xFDTD® tool, a commercially available time domain simulator using the finite-difference time domain method (FDTD) [24]. The software runs on a Dell Precision™ 7810 with 172 GB of memory, with numerical field simulations using two Nvidia® K20 Tesla® GPU accelerators. The generation and meshing of the structure do not utilize the GPUs.

As shown in Fig. 1, an EM plane wave is applied from the $-x$ direction. The waveform of the excitation signal is a 16.5 GHz sinusoid. This microwave frequency is chosen based on previous investigations which considered initiation of energetic materials with EM excitation [1]. The magnitude of the electric field is 1 MV/m, somewhat less than the breakdown field strength in air of approximately 3 MV/m. Neither the RDX inclusions nor the estane binder are magnetic materials, and there is no evidence suggesting that magnetic fields influence initiation. The recorded data is therefore limited to the electrical field response of the system. The duration of the EM simulation is four periods of the sinusoid (245 ps), and the electric field is recorded at all points on the mesh at a polling interval of less than 1/7$^{\text{th}}$ the period of the excitation, 8.3 ps.

The simulation space is terminated in absorbing boundary conditions implemented using the perfectly matched layer method, at distances from the scattering medium equal to the medium's dimensions.

C. METHODS-THERMAL

The thermal simulation, implemented in MATLAB®, is performed separately from the EM simulation. A uniform initial temperature of 300 K is assumed throughout the medium. The field values recorded from the EM simulation are used to determine the electric heating response of the medium through the dielectric heating equation (assuming magnetic effects are negligible):

$$\frac{dQ}{dt} = \omega \cdot \varepsilon_0 \cdot \varepsilon_{r,\text{imag}} \cdot E^2 \tag{1}$$

where $\frac{dQ}{dt}$ is the rate of heating per unit volume, ω is the angular frequency of the EM wave, $\varepsilon_{r,\text{imag}}$ is the imaginary relative permittivity of the material, ε_0 is the free-space permittivity, and E is the instantaneous electric field strength in V/m. Thermal diffusion is incorporated using the heat conduction equation:

$$\rho c_p \frac{dT}{dt} = \nabla \cdot (\kappa \nabla T) + \frac{dQ}{dt} \tag{2}$$

where T is the temperature, ρ is the material density, c_p is the specific heat of the material, and κ its thermal conductivity. To accommodate the grid-like mesh of the FDTD-based EM simulator, the Laplacian in (2) is realized in its 3D finite difference cartesian form.

Outside the scattering volume, it is assumed that there is no conduction of heat. At the boundaries of the simulation space, the Laplacian becomes a single-sided differential in the direction of the boundary. This method of termination is

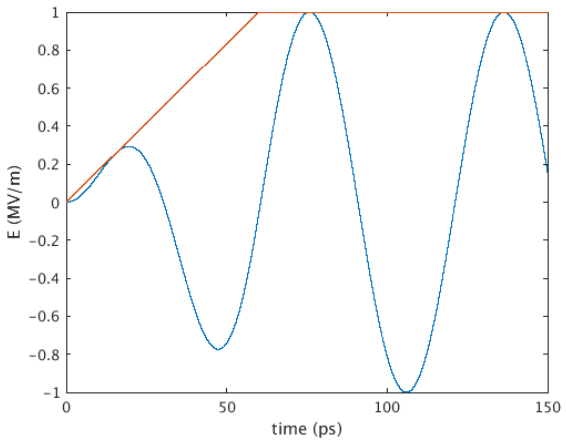

FIGURE 2. Windowed sinewave showing the first two cycles of the excitation, with the envelope window in red.

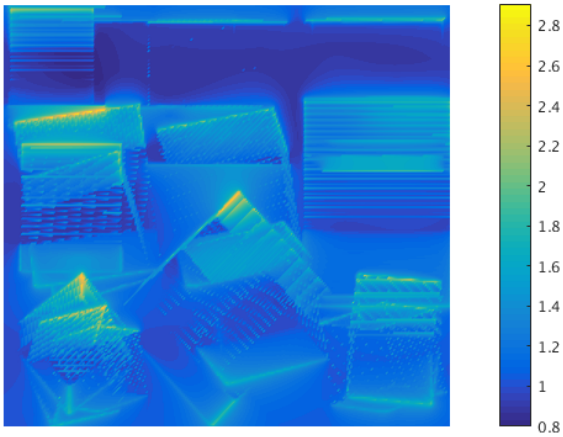

FIGURE 3. Cross section of peak electric field strength in MV/m, maximum value over x projected onto the y-z plane.

chosen to account for the structure being a part of a larger batch of material.

D. METHODS-EM THERMAL COUPLING

The total duration of the EM simulation is four RF cycles (245 ps), too short an exposure to generate a significant change in temperature. This limitation results from the fineness of the EM mesh required to achieve the necessary spatial and temporal resolution leading to very large data sets. The excitation must be windowed to be physically realizable, as illustrated in Fig. 2, and so the response during the time of the first cycle is ignored due to startup effects. The response of the last cycle is ignored as well. This leaves two cycles (122 ps) of electric field data to represent the EM response of the medium, which are repeated for the duration of the thermal simulation – previous results have shown the field response to remain stable after the initial buildup [21]. The EM-thermal analysis also assumes that the permittivity of the medium is independent of temperature. Recent investigations have shown dielectric properties of HMX (a similar energetic material) to remain relatively constant [16], [25]. The real permittivity, which is several orders of magnitude higher than the imaginary component, has been shown to vary by less than 1% between temperatures of 300 K and 400 K [22].

The EM simulation timescale is much finer than is necessary to accurately model thermal conductivity. Attempting to perform the thermal simulation at the time resolution of the EM process would result in exorbitant runtimes. To perform the simulation within a reasonable timeframe and maintain accuracy, the thermal conduction simulation is updated only once every 2000 RF cycles (122 μs). The dielectric heating is updated at every timestep. In (2), $\frac{dT}{dt}$ is updated once every 2000 RF cycles using the instantaneous value of T, while $\frac{dQ}{dt}$ is evaluated using (1) at every timestep of the EM simulation. To adjust for the difference in timestep lengths in the evaluation of the dielectric and conduction heating equations, the dielectric heating rates for each RF cycle integrated over 2000 RF cycles.

In the simulations reported here, peak memory usage was 150 GB during meshing, and this memory is also required by the virtual disk during post-processing of results. Typical runtimes is 70 minutes for the EM simulation and 18 hours for the thermal simulation.

IV. EM RESULTS

Fig. 3 illustrates the peak electric field data recorded in the EM simulation. To represent the entire 3D medium in a two-dimensional image, the values on the color plot represent the maximum instantaneous electric field over the x dimension (direction of wave propagation), and the time period of the recording (122 ps). The maximum instantaneous value of the electric field magnitude at any location is 2.91 MV/m, with a mean value of 0.88 MV/m. The maximum field magnitudes are recorded in the RDX crystal, where the mean peak field is 0.73 MV/m. In the binder, the maximum peak field magnitude is 2.24 MV/m, with a mean value of 0.97 MV/m. The discrepancy between the relative maximum and mean values is attributed to fields which may be very high at the surface of inclusions, but decrease substantially into the material. The peak fields occur at the edges of individual inclusions, and the area of localization spreads over the RDX-binder interface. That is, the maximum fields in both the RDX and binder are observed at these corners and edges of inclusions.

In addition to the role that the electric field plays in the dielectric heating process, it also produces instability in chemical bonds. This has been shown to combine with thermal, acoustic and mechanical stresses to lower the overall threshold for initiation [2], [5], [10]. Such bond weakening could intensify the impact of the increased temperatures caused by dielectric heating relative to similar changes in temperature caused by non-EM sources.

V. THERMAL RESULTS

The dielectric heating density from (1) is integrated over the two RF cycle (122 ps) duration of the EM simulation to obtain the heat transfer due to dielectric loss over two periods of

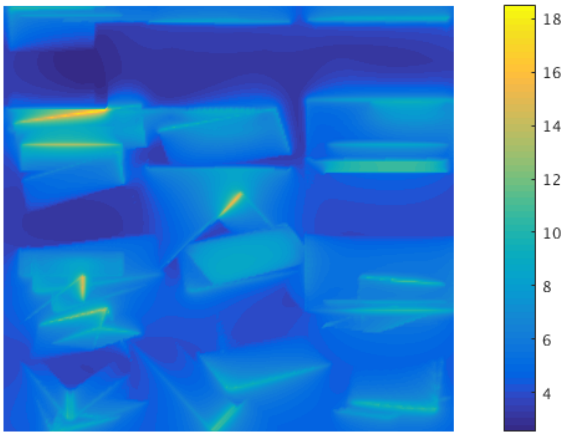

FIGURE 4. Cross section of heat transfer density over two periods of excitation sinusoid in J/m^3, maximum value over x projected onto y-z plane.

sinusoidal excitation. This is shown in the color plot in Fig. 4. Similar to Fig. 3, the values on the color plot represent the single point of maximum heat transfer over the x dimension (direction of wave propagation).

Over two RF cycles, the maximum heating observed is 18.52 J/m^3, with a mean value of 2.695 J/m^3. The maximum heat change occurs in the binder, where the mean value is 3.94 J/m^3. In the RDX crystal, the maximum is 7.724 J/m^3, while the mean is only 0.558 J/m^3. Despite the high field values in the crystal, its relatively small dielectric loss coefficient results in lower peak heating. It is apparent through examination of Figs. 2 and 3 that the electric field peaks and heat transfer peaks mostly align, due to the presence of relatively high fields in the binder near the electric field peaks just inside the crystal inclusions. The locations of maximum heat generation are shown to be at or near the edges of crystals.

VI. HOTSPOT TRACKING

The thermal simulator is run for 60 million RF cycles (3.7 ms) and implements (1) and (2), with (1) updating each cycle and (2) updating every 2000 RF cycles. The key result is that there were five locations which eventually had significantly higher than average temperatures. The five locations tracked are circled in Fig. 5(a).

Figs. 5–8 were developed using the same method as Figs. 3 and 4, where the color represents the maximum temperature over the x dimension (projected in the y-z plane).

After 1 million cycles it is observed that most of the peak electric field localizations in Fig. 3(a) align with the temperature peaks in Fig. 5(a). Locations 1 and 2 show the highest temperature, with increases of 2–3 degrees over the initial 300 K. Locations 3 and 5 show only a slightly lower temperature than 1 and 2. Location 4 at this point shows mild and unfocused heating. Examining the conduction heat transfer map in Fig. 5(b), the locations with the highest conducted heat flux are in the proximity of the temperature peaks.

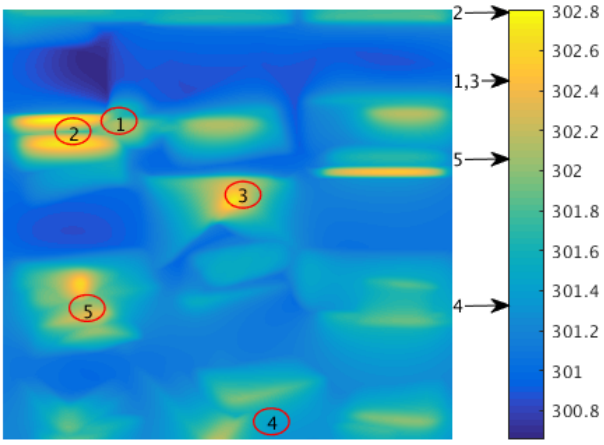

(a)

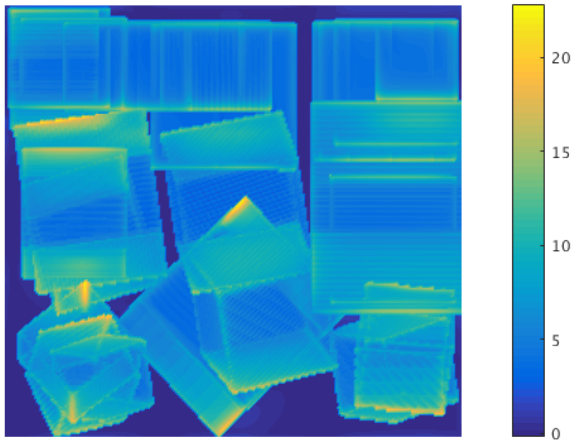

(b)

FIGURE 5. Thermal status at 1 million cycles (60.6 μs) projected in the y-z plane: (a) temperature in kelvin; and (b) temperature change due to conduction in K/μs. The circles in (a) identify five locations of interest over the course of the simulation.

This, along with the clear delineation between the crystal and the binder and the observation that the heat transfer on the crystal side is much higher, supports the conjecture that the highest temperatures are occurring in the binder in the proximity of the electric field peaks. It is also at the binder-crystal interface where the half molecules of RDX, which have low stability, are to be found.

After 5 million cycles, see Fig. 6, the dominance of locations 1 and 2 has faded, and location 5 has taken over as the area of highest temperature. Location 4 still displays relatively measured temperature change. The conduction map shows similar behavior to the Fig. 5, though thermal conduction is now occurring throughout the medium, as opposed to being limited to areas near high electric fields at the earlier timestep. One noticeable change is a blurring of lines over the whole structure of Fig. 6(a), suggesting that the conduction is taking effect, even though the plot of conducted heat flow, Fig. 6(b), appears to be similar.

After 15 million cycles, see Fig. 7, the temperature peaks at locations 1 and 2 are diminished and no longer discernible

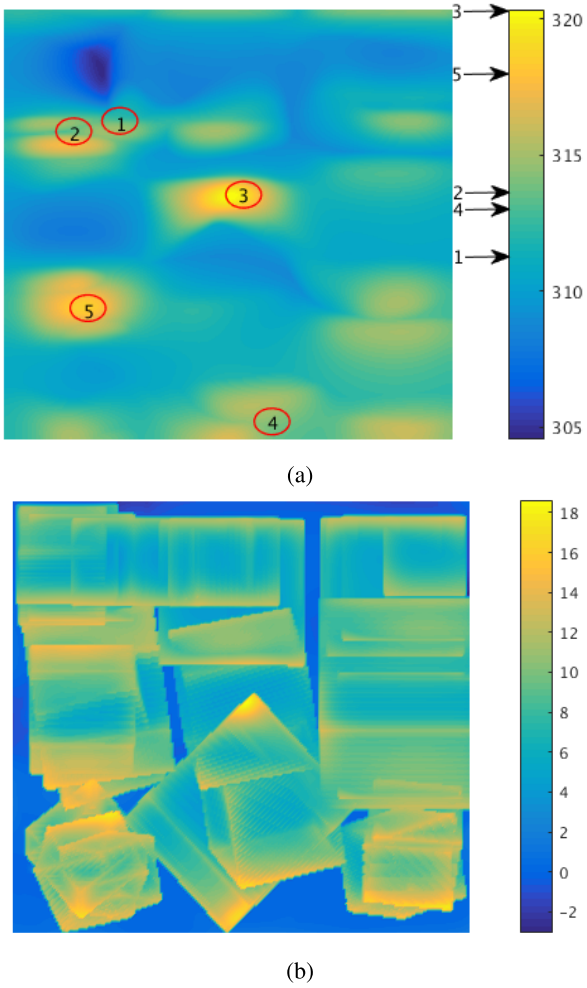

FIGURE 6. Thermal status at 10 million cycles (606 μs) projected in the y-z plane: (a) temperature in kelvin; and (b) temperature change due to conduction in K/μs. The circles in (a) identify five locations of interest over the course of the simulation.

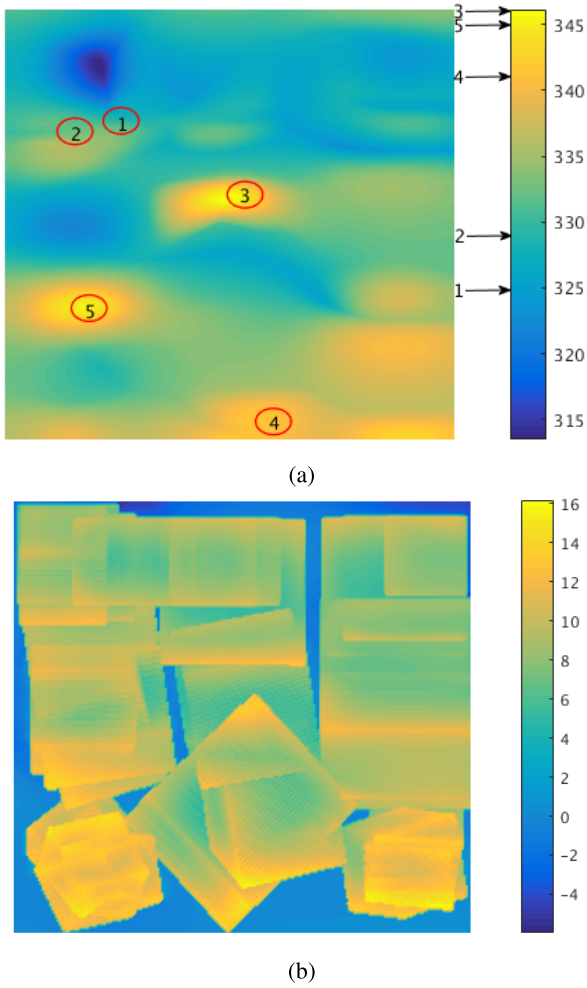

FIGURE 7. Thermal status at 30 million RF cycles (1.82 ms) projected in the y-z plane: (a) temperature in kelvin; and (b) temperature change due to conduction in K/μs. The circles in (a) identify five locations of interest over the course of the simulation.

from each other, now forming a small pocket of slightly above average temperature. Heating due to thermal conduction in the inclusions towards the bottom of the figure is beginning to increase.

After 30 million cycles, see Fig. 8, the high heating in the high binder concentration regions near location 4 dominates and is now the region of highest temperature in the entire medium, with locations 3 and 5 within 5 K. Locations 1 and 2 are much lower in temperature. Most of the heat is generated in the binder due to its relatively high dielectric loss, and the regions of highest heat conduction (near the bottom of the cross section here) are those with the lowest RDX density.

From Figs. 5–8, it is observed that relatively small regions of RDX crystals have high heating due to high electric field values at the corners of these crystals as well as in the surrounding binder. From the conduction plots, it is apparent that the diffusion of heat from the surrounding binder plays a significant role in creating the high temperatures found at these corners.

Overall, the binder displays higher temperatures by the completion of the 60 million RF cycles. High temperatures in the binder are not limited to the corners of the RDX-binder interface and occur over larger areas. This is due to the higher dielectric loss of the binder, as well as the lower loss through diffusion. Binder dense regions receive dielectric heating throughout, leading to lower temperature gradients compared to the corners of crystals, where the crystal interiors experience very little dielectric heating, and much larger temperature gradients exist.

BEHAVIOR WITHIN INCLUSIONS

While Figs. 5–8 were chosen to best display the gradual change of temperature throughout the medium, they do not show the thermal behavior within an individual inclusion. Specifically, taking the maximum temperature in the x direction obscures the lower temperatures within the inclusions. Fig. 9 is a cross section at a single value of x rather than a maximum over the whole range of x, the temperature profile

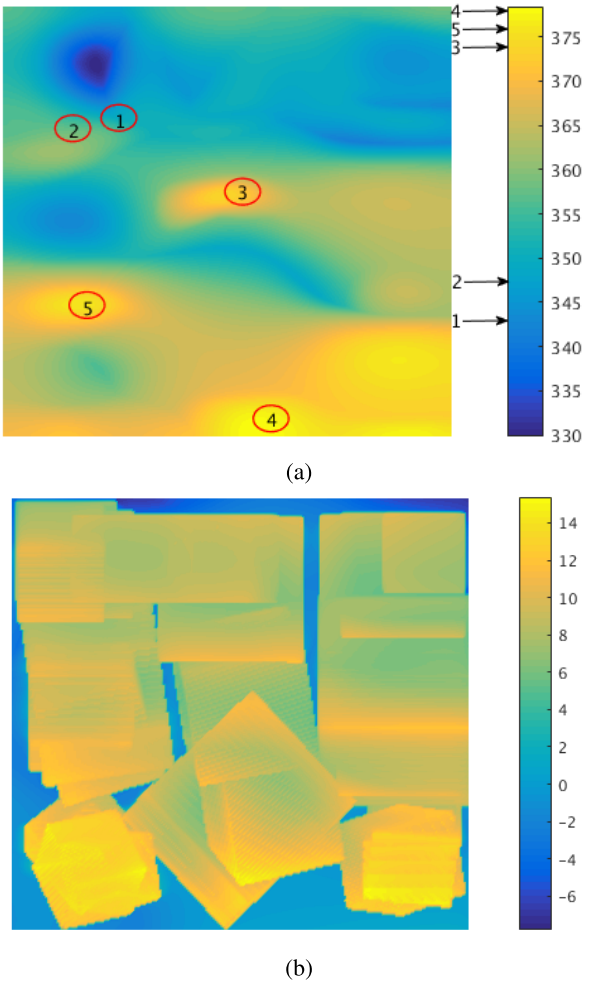

FIGURE 8. Thermal status at 60 million RF cycles (3.64 ms) projected in the y-z plane: (a) temperature in kelvin; and (b) temperature change due to conduction in K/μs. The circles in (a) identify five locations of interest over the course of the simulation.

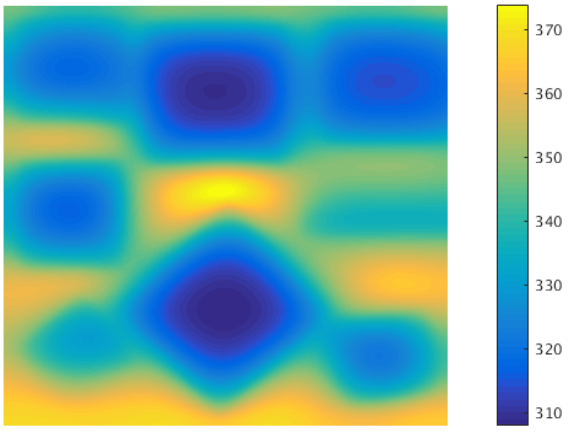

FIGURE 9. Single cross section in the y-z plane after 60 million RF cycles, showing the cold interior of inclusions.

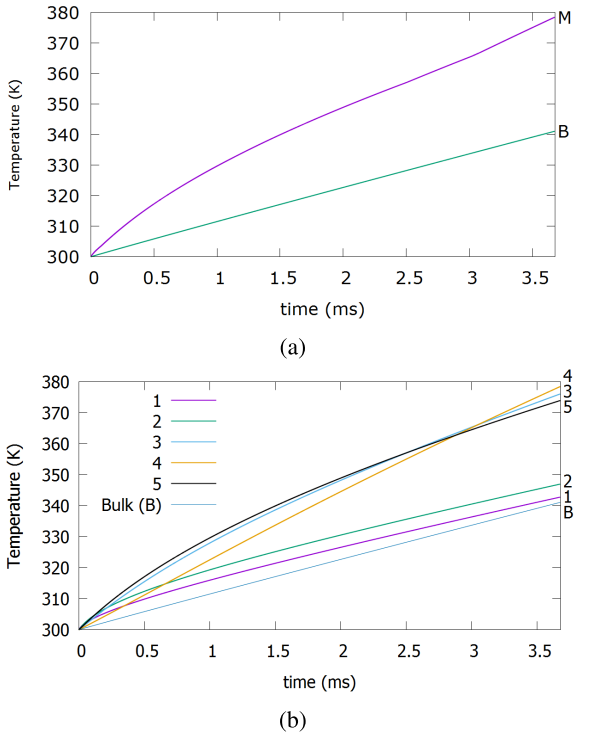

FIGURE 10. Absolute temperature (a) maximum (M) and average bulk (B) temperature across entire medium; (b) and at five locations of interest, average temperature (B) across structure for comparison, recorded over entire simulation.

shown in Fig. 9 is that at 30 million cycles. There is a monotonic decrease in temperature below the surface of the inclusions, with larger inclusions having the lowest temperatures in the entire medium. The conduction heating from the high temperatures at the surface of inclusions is unable to penetrate very far into the inclusion. While the inclusions are adjacent to the binder where the great majority of the heat is generated, high volumes of material inside the inclusions receive very little dielectric heating, leading to relatively low temperature increase inside the inclusions.

VII. GRAPHS

The previous section tracked temperature profiles using color contour plots at several specific times. To supplement this, Fig. 10 shows the temperature transients at the five locations of interest previously identified. These five locations, see Figs. 5–8, showed temperatures at or near the maxima within the medium for a significant portion of the time considered. The mean temperature of the entire system, henceforth referred to as the bulk temperature, is included for comparison.

The local geometries of the locations tracked in Figs. 5 – 8 are shown in Fig. 11, where the yellow shading represents RDX and blue represents the binding polymer. Locations 1 and 2 are within 50 μm of each other, each being where two inclusions come in close proximity at an angle. These two locations also correspond to the regions of highest field localization shown in Fig. 3. Locations 3 and 5 are regions where inclusions are relatively close to each other, but not

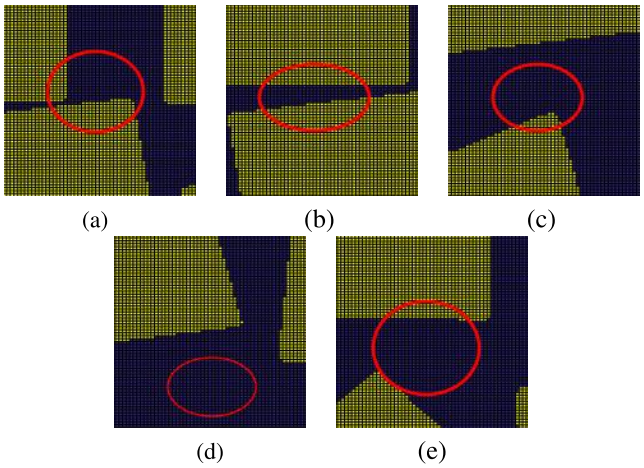

FIGURE 11. Local geometries of locations 1–5.

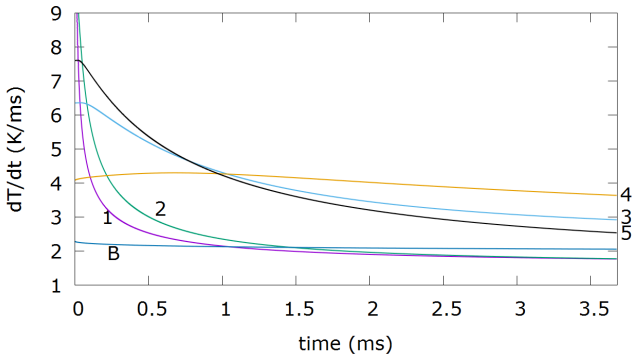

FIGURE 12. Total heating rate at each location with the bulk heating rate for comparison.

quite to the degree of the first two. Location 4 is in a relatively loosely packed region consisting mostly of binder.

The regions with inclusions in close proximity, locations 1 and 2, exhibit high rates of heating, as shown in Fig. 12(b). These rates drop quickly, approaching that of the bulk heating rate. Locations 3 and 5, which have a relatively low density of RDX crystal, have a faster temperature increase, falling to half the initial rate after 1.22 ms, compared to approximately 0.78 ms for location 1 and 0.49 ms for location 2. Meanwhile location 4 has the highest concentration of binder and shows the most constant rate of temperature increase.

The differing behaviors at these locations is due to the relative levels of dielectric heating and heat transfer via conduction, see Fig. 13. Since dielectric heating is constant, as the incident field and physical parameters remain unchanged over the 60 million RF cycles, this comparison effectively realizes as Fig. 12.

Thermal conduction counters the temperature rise resulting from dielectric loss such that regions with high RDX density display a slower increase in temperature than regions with lower RDX density. The RDX crystals with their higher thermal conductivity act as a heatsink for the heat generated in the

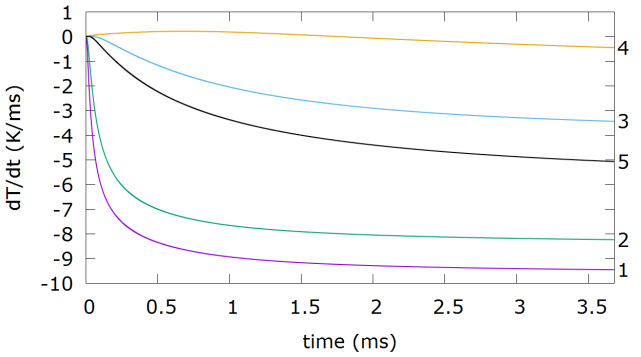

FIGURE 13. Conduction heating rate at each location of interest.

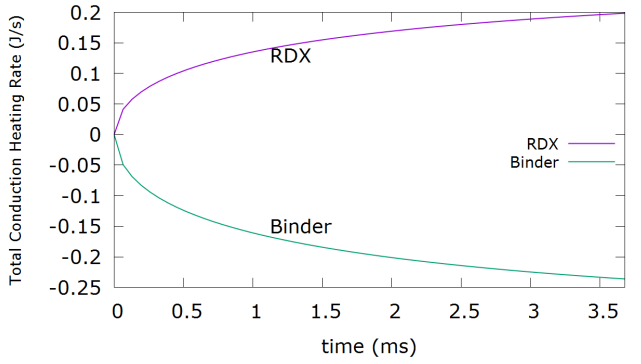

FIGURE 14. Total heating rate of RDX and binder due to conduction over entire simulation.

binder. This is observed in Fig. 14, where the total conduction heating rate is plotted for the RDX and the binder, and shows energy consistently moving from the binder into the RDX. This is partially due to RDX having lower dielectric loss and therefore lower dielectric heating, but also because the product of the specific heat and density of RDX is higher than that of the binder. Thus, for the same heating the temperature rises more slowly in RDX.

DISTRIBUTION

Fig. 15 displays a histogram of the final distribution (after 30 million cycles) of temperatures in the medium within the RDX and binder. Overall, the binder temperatures are substantially higher than that of the RDX crystals. The RDX temperature distribution is smooth, while the variation in the binder is believed to be due to the often very small regions between RDX crystals, which receive high dielectric heating from the edge-enhanced fields. This is supported by the behavior shown in Fig. 9 and the locations of the hotpots.

VIII. DISCUSSION

Based on these observations, a working hypothesis is constructed as follows. The highest electric field peaks occur in regions where there is high packing density of inclusions, resulting in a large number of corners and edges. This has been demonstrated before [17], [21]. However, as heating is more efficient in the binder, the regions with the highest

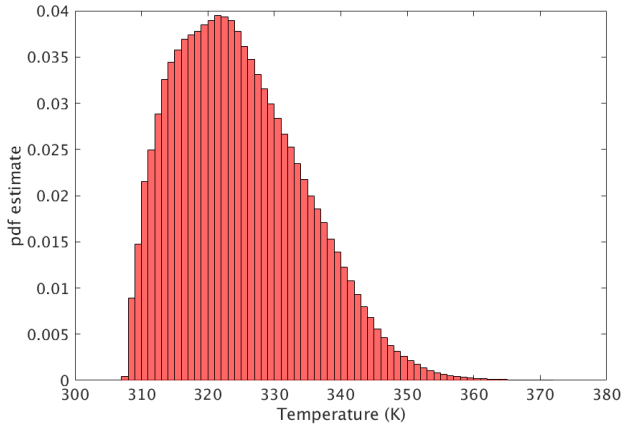

(a)

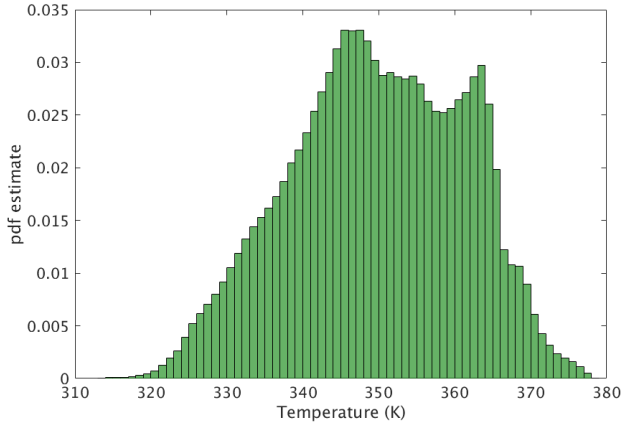

(b)

FIGURE 15. Histograms of temperature distribution in (a) RDX and (b) binder at end of simulation, each division in the x–axis is 1 kelvin.

density of the binding material eventually become the locations of highest temperature. During the transition time between the two extremes, the regions of highest temperature occur where there is a balance of binder and features that induce field-localization, i.e. the edges and corners of inclusions. The highest temperatures in the RDX inclusions are at the surfaces of, and particularly at edges and corners of inclusions.

Fig. 9 shows that the inner portions of the RDX inclusions remain at relatively low temperatures, even though the high temperature difference compared to the surface should cause high levels of heat flow towards the interior due to conduction. This shows that the conduction heating progresses very slowly relative to the dielectric heating. High temperature gradients are possible, although the areas of low temperature must be far from the binder, as the temperatures in the binder will be high to its higher heating efficiency.

For relatively loosely packed mediums, such as the one in this work, the presence of binder throughout the medium results in relatively quick bulk heating. For highly packed energetic materials with binder volume fractions below 10%, typical of military-grade explosives, bulk heating would be less significant.

The 65 K peak temperature increase in the RDX, as seen in Fig. 15(a), is at the surface of inclusions and is believed to be sufficiently close to the temperature rise required to initiate deflagration [3], [16]. The likelihood increases when combined with the high electric fields that occur at the edges and corners of inclusions as the high temperatures reduce the breakdown strength of a molecule. The highest temperatures and peak electric fields generally coincide at the surface of an inclusion and, importantly, it only requires one molecule or half-molecule to breakdown for a chain reaction to be initiated.

IX. CONCLUSIONS

The sinusoidal excitation used in this study possessed an incident electric field magnitude of 1 MV/m, which is equivalent to an incident EM wave with a power density of 1.3 GW/m^2. While this is sustainable for a few nanoseconds [15], it is not sustainable for the nearly 4 ms required here to achieve a temperature rise of 65 K in the RDX crystal and 75 K in the binder. A reduced incident field strength of 1 MW/m^2 could possibly achieve similar levels of heating, but the long exposure time necessary would render such a system ineffective for threat detection/neutralization over large areas. Thus, the mechanisms for a feasible neutralization system must be due to the occurrence of high peak fields in the explosive, and not the heating induced. The breakdown strength of RDX molecules is known to be 12–18 MV/m and the peak fields determined in this study approaching 3 MV/m. The RDX half molecules on the surfaces of RDX inclusions are known to be much less stable than that of a whole molecule. The breakdown strength of half molecules is unknown but should be many times less than that of a whole RDX molecule. Thus, it should be possible to design a microwave system to neutralize improvised explosives. The high incident field strengths could be produced by standoff generators [15] or by a spark gap generators placed in close proximity to a suspicious object.

REFERENCES

[1] K. Hasue, M. Tanabe, N. Watanabe, S. Nakahara, F. Okada, and A. Iwama, "Initiation of some energetic materials by microwave heating," *Propellants, Explosives, Pyrotech.*, vol. 15, pp. 181–186, Oct. 1990.
[2] S. Ahmad and D. Russell, "Laser ignition of pyrotechnics—Effects of wavelength, composition and confinement," *Propellants, Explosives, Pyrotech.*, vol. 30, no. 2, pp. 131–139, 2005.
[3] W. Perry and A. Higginbotham-Duque, "Micro to mesoscale temperature gradients in microwave heated energetic materials," *J. Appl. Phys.*, vols. 5–116, p. 054911, Aug. 2014.
[4] A. Ali, M. Sandstrom, D. Oschwald, K. Moore, and S. Son, "Laser ignition of DAAF, DHT and DAATO3.5," *Propellants, Explosives, Pyrotech.*, vol. 30, no. 5, pp. 351–355, 2005.
[5] J. S. Murray, M. C. Concha, and P. Politzer, "Links between surface electrostatic potentials of energetic molecules, impact sensitivities and C-NO_2/N-NO_2 bond dissociation energies," *Molecular Phys.*, vol. 107, no. 1, pp. 89–97, 2009.
[6] J. S. Murray, P. Lane, and P. Politzer, "Relationships between impact sensitivities and molecular surface electrostatic potentials of nitroaromatic and nitroheterocyclic molecules," *Molecular Phys.*, vol. 85, no. 1, pp. 1–8, 1995.

[7] M. A. Wood, A. C. T. van Duin, and A. Strachan, "Coupled thermal and electromagnetic induced decomposition in the molecular explosive αHMX; a reactive molecular dynamics study," *J. Phys. Chem. A*, vol. 118, no. 5, pp. 885–895, 2014.
[8] J. Brown and M. Zikry, "Effect of microstructure on the coupled electromagnetic-thermo-mechanical response of cyclotrimethylenetrnitramine-estane energetic aggregates to infrared laser radiation," *J. Appl. Phys.*, vol. 118, p. 124902, Sep. 2015.
[9] M. Williams and M. Matei, "The decomposition of some RDX and HMX based materials in the one-dimensional time to explosion apparatus. Part I. Time to Explosion and Apparent Activation Energy," *Propellants, Explosives, Pyrotech.*, vol. 31, no. 6, pp. 435–441, 2006.
[10] E. D. Aluker, A. G. Krechetov, A. Y. Mitrofanov, A. S. Zverev, and M. M. Kuklja, "Understanding limits of the thermal mechanism of laser initiation of energetic materials," *J. Phys. Chem. C*, vol. 116, no. 46, pp. 24482–24486, 2012.
[11] H. OÖstmark, M. Carlson, and K. Ekvall, "Concentration and temperature measurements in a laser-induced high explosive ignition zone. Part I: LIF spectroscopy measurements," *Combustion Flame*, vol. 105, no. 3, pp. 381–390, 1996.
[12] S. D. McGrane and D. S. Moore, "Continuous wave laser irradiation of explosives," *Propellants, Explosives, Pyrotech.*, vol. 36, no. 4, pp. 327–334, 2011.
[13] C. Matzler, "Microwave permittivity of dry sand," *IEEE Trans. Geosci. Remote Sens.*, vol. 36, no. 1, pp. 317–319, Jan. 1998.
[14] N. R. Peplinski, F. T. Ulaby, and M. C. Dobson, "Dielectric properties of soils in the 0.3–1.3–GHz range," *IEEE Trans. Geosci. Remote Sens.*, vol. 33, no. 3, pp. 803–807, May 1995.
[15] H. Zhang, T. Shu, J. Ju, and D. Wu, "Gigawatt-class radiation of TM_{01} mode from a KU-band overmoded cerenkov-type high-power microwave generator," *IEEE Trans. Plasma Sci.*, vol. 42, no. 6, pp. 1567–1572, Jun. 2014.
[16] B. B. Glover, M. E. Daily, S. F. Son, and L. J. Groven, "X-Band microwave properties and ignition predictions of neat explosive," *Propellants, Explosives, Pyrotech.*, vol. 38, pp. 810–817, Dec. 2013.
[17] A. Pickles and M. Steer, "Electromagnetic properties of disordered three-dimensional mixtures," *IEEE Access*, vol. 1, pp. 778–788, 2013.
[18] A. Pickles, I. Kilgore, and M. Steer, "Automated creation of complex three-dimensional composite mixtures for use in electromagnetic simulation," *IEEE Access*, vol. 1, pp. 248–250, 2013.
[19] D. Mathieu, "Theoretical shock sensitivity index for explosives," *J. Phys. Chem. A*, vol. 116, no. 7, pp. 1794–1800, 2012.
[20] B. Asay, *Non-Shock Initiation of Explosives*, vol. 5. Springer, 2010.
[21] M. Chen and M. Steer, "Abstracted random mediums for electromagnetic hotspot observation in finite difference time domain simulation," *IEEE Trans. Microw. Theory Techn.*, vol. 65, no. 5, pp. 1873–1879, May 2017.
[22] W. Kort-Kamp *et al.*, "Microscale electromagnetic heating in heterogeneous energetic materials based on x-ray computed tomography," *Phys. Rev. Appl.*, vol. 5, no. 4, p. 044008, 2016.
[23] G. Cawsey, J. Farrands, and S. Thomas, "Observations of detonation in solid explosives by microwave interferometry," *Proc. Roy. Soc. Lond.*, vol. 248, pp. 399–521, Dec. 1958.
[24] (2017). *xFDTD*. [Online]. Available: https://www.remcom.com/
[25] D. Reese, S. Son, and L. Groven, "Preparation and characterization of energetic crystals with nanoparticle inclusions," *Propellants, Explosives, Pyrotech.*, vol. 37, pp. 635–638, Nov. 2012.

MICHAEL CHEN received the B.S. degree in electrical engineering from Duke University and the M.S. and Ph.D. degrees in electrical engineering from North Carolina State University.

MOHAMMED A. ZIKRY received the B.S. from the University of Kansas, the M.S. degree from the Johns Hopkins University, and the Ph.D. degree from the University of California, San Diego. He is currently the Zan Prevost Smith Professor with the Department of Mechanical and Aerospace Engineering, North Carolina State University. He has been a Senior Research Advisor to the Army Research Office and a consultant to numerous industries. He is a fellow of the American Association for the Advancement of Science, the Society of Engineering Science, and the American Society of Mechanical Engineering (ASME). He has received the Jefferson Science Fellowship (Advisor to the Secretary of State, U.S. State Department), the Thurston Lecture Society Award from ASME, the Senior Research Fulbright Award, the R.J. Reynolds Award, the ALCOA Distinguished Research Award, the NCSU Research Excellence Award, and the Ralph Teetor Research Award from the Society of Automotive Engineering. He has also received the Alumni Award for Impact from the University of California, San Diego, and the Distinguished Alumni Award from the University of Kansas. He has been awarded a Professeur, Premiere Classe, at Strasbourg University. He was the Chair of the Executive Committee of ASME's Material's Division. He is the Editor-in-Chief of the *Journal of Engineering Materials and Technology* (ASME) and the Regional Editor of *Mechanics of Materials*.

MICHAEL B. STEER (F'99) was the Jack S. Kilby Lecturer in 2003. He is currently the Lampe Distinguished Professor of Electrical and Computer Engineering, North Carolina State University (NC State). He has authored over 485 refereed publications and four books. He was a member of the Microwave Theory and Techniques Society (MTT-S) Administrative Committee from 1998 to 2001 and from 2003 to 2006. He is an elected member of the Administrative Committee of the IEEE Microwave Theory and Techniques Society. He received Service Recognition Awards from the IEEE Microwave Theory and Techniques Society in 1998 and 2001. He received the Presidential Young Investigator Award in 1986 and the Alcoa Foundation Distinguished Research Award from the NC State's College of Engineering in 2003. In 1994 and 1996, he received the Bronze Medallion from the U.S. Army Research for Outstanding Scientific Accomplishment. In 2007, he received the Distinguished Service Recognition Award from the IEEE MTT-S. In 2009, he received an Army Medal, the Commander's Award for Public Service. He received the 2010 Microwave Prize for the best paper on Microwave Engineering in any IEEE publication in the preceding year. In 2011, he received the Distinguished Educator Award from the IEEE MTT-S. In 2013, he received the R.J. Reynolds Award for Excellence in Teaching, Research, and Extension from the College of Engineering, NC State University. In 2017, he received the Alexander Quarles Holladay Medal from NC State University. This is the highest award made by the university in recognition of faculty career achievements. He is a former Editor-in-Chief of the IEEE TRANSACTIONS ON MICROWAVE THEORY AND TECHNIQUES. He was the Secretary of the IEEE MTT-S in 1997. He was inducted into the Electronic Warfare Technology Hall of Fame sponsored by the Association of Old Crows. He was named one of the Most Creative Teachers in the South by *Oxford American*.